BENTHAM SCIENCE

CrossMark

Current Medical Imaging

Content list available at: https://benthamscience.com/journals/cmir

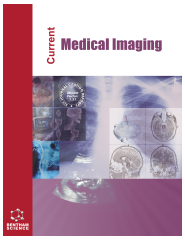

RESEARCH ARTICLE

Microwave Imaging: Locating Bone Fractures using Patch Antenna of ISM Band

Joselin Jeya Sheela John Bosco[1], Gul Shaira Banu Jahangeer[2], Duraichi Natarajan[1], Logeshwaran Murugavel[3,*] and Jeyapoornima Balasubramanian[1]

[1]*Department of Electronics and Communication Engineering, Saveetha School of Engineering, Saveetha Institute of Medical and Technical Sciences, Saveetha University, Chennai, India*
[2]*College of Computers and Information Technology, Taif University, Taif Kingdom of Saudi Arabia*
[3]*Department of Electronics and Communication Engineering, R.M.K. Engineering College, RSM Nagar, Kavaraipettai, Gummidipoondi Taluk, Tiruvallur -601206, Tamil Nadu, India*

Abstract:

Background:

The human skeletal system relies heavily on the integrity of bones, which provide structural support and safeguard vital organs. Accurate detection is paramount for effective diagnosis. Conventional methods for identifying fractures manually are not only time-consuming but also susceptible to errors.

Methods:

The proposed methodology hinges on a patch antenna operating at 2.4 GHz and a bone phantom housing a simulated fracture, where the antenna is scanned. The collected signals are then processed with Delay-and-Sum (DAS), and Delay-Multiply-and-Sum (DMAS) reconstruction algorithms. The resulting images offer visual insights into the location of fractures.

Results:

Through experimentation, the efficacy of the images varies considerably in terms of their capacity for noise and artifact suppression. While DAS exhibits reasonable effectiveness, it suppresses noise and artifacts comprehensively. In contrast, DMAS offers clearer and more precise images of bone fractures.

Conclusion:

In summary, the research introduces a cost-effective and non-invasive strategy for detecting bone fractures. By involving a patch antenna at 2.4 GHz, along with image reconstruction algorithms like DMAS and DAS, one can effectively visualize the location of bone fractures. The experimental results highlight the superiority of DMAS over DAS in terms of contrast resolution, making it a highly promising avenue for fracture detection.

Keywords: Industrial scientific medical band, Patch antenna, Bone fracture, Microwave imaging, Medical applications, Return loss, Delay-and-sum, Delay-multiply-and-sum.

Article History	Received: September 28, 2023	Revised: December 02, 2023	Accepted: December 07, 2023

1. INTRODUCTION

Bone is a crucial part of the human body. The potential to relocate the body is conferred by bone. Bone fractures are rather prevalent in humans [1]. It serves vital roles, for example, mineral storing, and mechanical strength, for soft tissues and organs. Our bodies are supported by bones, which help determine our shapes. Despite their low weight, bones are robust enough to sustain our complete body mass. Bone fractures might happen for several causes. Osteoporosis, triggered by Vitamin D deficiency, promotes bone fragility,

* Address correspondence to this author at the Department of Electronics and Communication Engineering, R.M.K. Engineering College, RSM Nagar, Kavaraipettai, Gummidipoondi Taluk, Tiruvallur -601206, Tamil Nadu, India; E-mail: logeshwaran25092@gmail.com

which may lead to bone fracture. Bone is a large determinant in accidents, and extensive bone fractures culminate in human mortality [2]. Tibia, often referred to as the shinbone, found in the lower leg, is the longest bone. There is a greater chance of a tibia fracture occurring. Tibia fractures are prevalent in youngsters, sportspersons, and aged people, and it can be hard to diagnose at first [3].

"X-rays, Computed Tomography-(CT), and Magnetic Resonance Imaging-(MRI)" are vital diagnostic and diagnostic methods for bone illnesses such as fractures and joint problems [4]. Nevertheless, each strategy has its own set of drawbacks. For example, fractures are frequently identified *via* X-rays [5], which are the quickest and simplest approach to examining bone injuries, especially fractures. Nevertheless, because this approach includes radiation and has the potential to cause harm, it raises serious concerns, particularly in the case of babies and pregnant women. Furthermore, X-rays only give partial information on muscles, tendons, and joints [6]. Regrettably, CT is a remarkably efficient imaging approach that produces higher-quality images of human organs, such as images of difficult fractures, subtle cracks, or misalignments. Nevertheless, like with X-rays, ionizing radiation is a critical challenge with this technology, which restricts its applicability. Being expensive cost, CT and MRI are typically recommended when X-rays do not offer adequate details [7]. However, MRI offers a higher cost and time-consuming diagnosis. As per the guidelines of the World Health Organization (WHO), prolonged exposure of the human body to continuous radiation has the potential to induce cancer [8].

Elderly people and kids are more susceptible to falling and sustaining fractures. Tibia fractures stand as the third-most predominant long bone fracture in children, accounting for 15% of whole fractures [9]. Given the prevalence of fracturing in superficial bones, it is advantageous to have a non-ionizing and non-invasive screening approach. Despite different imaging technological advances, microwave imaging is regarded as appealing for diagnostic purposes due to its ability and safety in producing pictures of human organs [10]. Due to the discrepancy in microwave frequencies among the dielectric characteristics of healthy tissue and tissues with lesions, microwave imaging can be employed for the identification and monitoring of a range of disorders [11]. In sectors that include electronics to industrial, microwave non-invasive testing discovers flaws quicker and simpler [12]. Current years have seen a major increase in interest in the use of planar microwave sensors, for nondetrimental technique testing [13]. These sensors are not only able to pick up deep subterranean flaws, but they are also unobtrusive. Formerly, cumbersome waveguide components were employed for testing. For spotting flaws in materials, Horn antennas, and Open-ended rectangular waveguides remained deployed. Microwave sensors with printed transmission lines and patch antennas have been used in the last 10 years to monitor and measure the dielectric properties of substances [14]. Microwave imaging methods have piqued the interest of researchers, owing to their numerous advantages, including the utilization of non-ionizing signals, cheap cost, less intricacy, and capacity to penetrate deep through diverse media (air, skin, bones, and tissues [15]).

Various researchers have proposed diverse methods for monitoring at both lower and higher frequencies, including the development of a compact microwave device designed for fracture diagnosis [16]. This method utilizes the Lanczos imaging technique to visualize fractures by leveraging the transmission characteristics of a microwave ring resonator. The reported sensor, operating at 2.45 GHz, encounters challenges such as the loss of high-frequency contents during image restoration, leading to blurring in the final image. Another instance involves a UWB textile antenna operating in the 1.198–4.055 GHz range for biomedical applications [17]. However, this antenna is not low-profile, and there is a lack of an adequate detection system for image reconstruction to monitor internal damage beneath the skin. In a different approach, a planar monopole antenna was developed for detecting bone cracks or voids [18]. The system relies on a shift in the resonance frequency of the antenna to identify such issues. The challenge with this system lies in its large size, making it difficult to incorporate into a portable microwave system. Additionally, a smart bone plate designed for monitoring fracture healing was introduced [19], utilizing electrical impedance spectroscopy to monitor tissue healing. However, this system relies on impedance variation, introducing limitations in its application.

The process of forming images includes shining electromagnetic radiation onto a tissue and examining the signals reflected, scattered, or, at times, transmitted from dielectric boundaries within the tissue. Various signal processing methods have been suggested to generate an image. These algorithms can be broadly classified into two categories: one that aims to detect the presence and location of notable dielectric scatterers in the tissue (referred to as Radar approaches) and another that endeavors to reconstruct the complete dielectric profile of the examined tissue (referred to as tomographic approaches) [20]. The study [21] evaluates the performance of the imaging technique in scenarios of bone marrow lesions and bone fractures. It introduces parameters such as resolution and signal-to-clutter ratio (SCR) to quantify the imaging results. The impact of varying frequencies and bandwidths on image quality is explored, and the effectiveness of artifact removal techniques is assessed. A study [22] describes the method for tumor detection using high-frequency electromagnetic waves and Ground Penetrating Radar (GPR) algorithm with the Depth Migration Principle. The process involves focusing high-frequency electromagnetic waves on a head phantom, collecting backscattered reflections with a receiving antenna, and calculating the depth of the tumor. The GPR algorithm utilizes the two-way travel time (tR) of electromagnetic waves, considering reflections, refraction, diffraction, and reverberation until the waves become weak due to high target conductivity. An article [23] introduces an enhanced two-stage image inpainting network to address common issues like blurring, texture distortion, and semantic inaccuracies in existing algorithms. The method employs a parallel network with contextual attention for improved inpainting results. In the first stage, a deep residual network fills missing pixels, and an adversarial network enhances edge information. In the second stage, color features are extracted, edge maps are fused and complemented, and the fusion map

serves as a conditional label for the second-stage adversarial network. This approach [24] combines Semantic Priors, Deep Attention Residual Group, and Full-scale Skip Connection for enhanced authenticity and flexibility in handling missing and non-missing regions. The Semantic Priors Network captures comprehensive semantic information of visual elements in the gaps, aiding accurate [restoration. The Deep Attention Residual Group enables adaptive feature learning, emphasizing both missing regions and channel-specific details. Full-scale Skip Connection merges low-level and high-level feature maps, effectively repairing missing regions.

Thus, a design of a low-profile ISM band rectangle-shaped antenna for crack/fracture detection in bone is offered. The antenna is simulated, and antenna aspects are examined. For the analysis, a bone phantom with and without cracks is built into the software. At last, a real phantom is being tested, and the differences in return loss are being investigated. The collected data has been processed with the image reconstruction algorithms, and the processed image reveals the exact location of the bone fracture. Owing to a variety of characteristics, including their small size, smaller weight, low production costs, and adaptability to be combined with solid-state devices, patch antennas constitute one of the types of antennas that are deemed essential in wireless systems [25]. It is a type of narrowband antenna that is constructed from a flat rectangular metal sheet that is affixed to the top layer of a sheet of metal, recognized as the ground surface [26]. Radiating patches can have shapes like squares, rectangles, circles, ellipses, or other shapes. The most prevalent shapes are square, rectangular, and circular because of their simplicity in manufacturing and analysis [27]. Thus, on one side of the Dielectric substrate, Patch Antenna has a Ground plane and a Radiating patch on the other side. Copper is utilized to create patch layers. The dielectric constant-(εr) of the substrate's range is commonly between $2.2 < \varepsilon r < 12$ range. This study designs a patch Antenna of the ISM band, resonating at 2.4GHz. ISM bands, often referred to as "industrial, scientific, and medical" bands, have indeed been authorized for employment in implantable medical communication services by the "International Telecommunication Union-(ITU)" [28]. The overall dimensions of the patch antenna are 39.36 x 47.97 x 1.6 mm^3, as depicted in Fig. (**1**). The substrate is made of FR-4 (Lossy), with dielectric constant-(εr) of 4.4, and copper (pure), and the antenna is fabricated, and depicted in Fig. (**2**). The antenna dimensions are calculated as per the study [29].

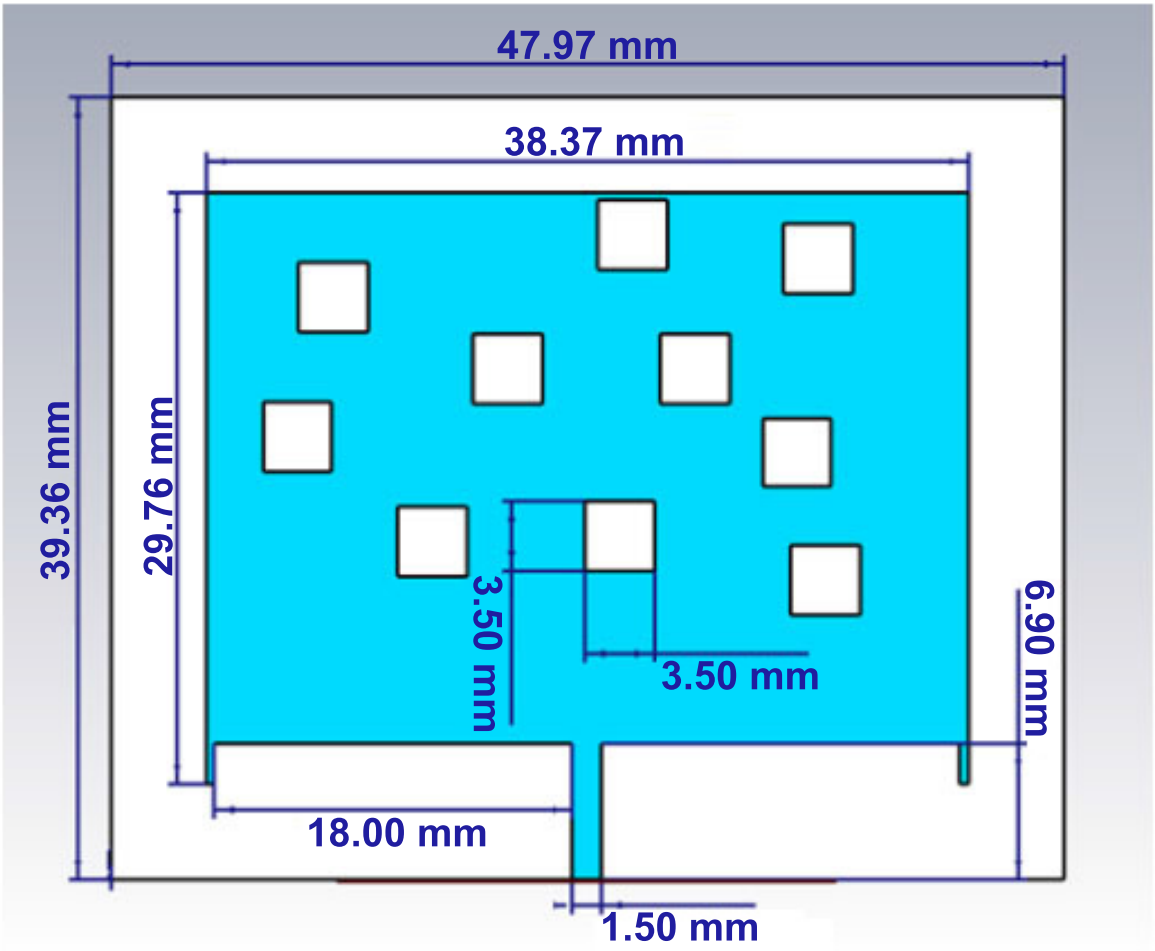

Fig. (1). Antenna design for 2.4GHz.

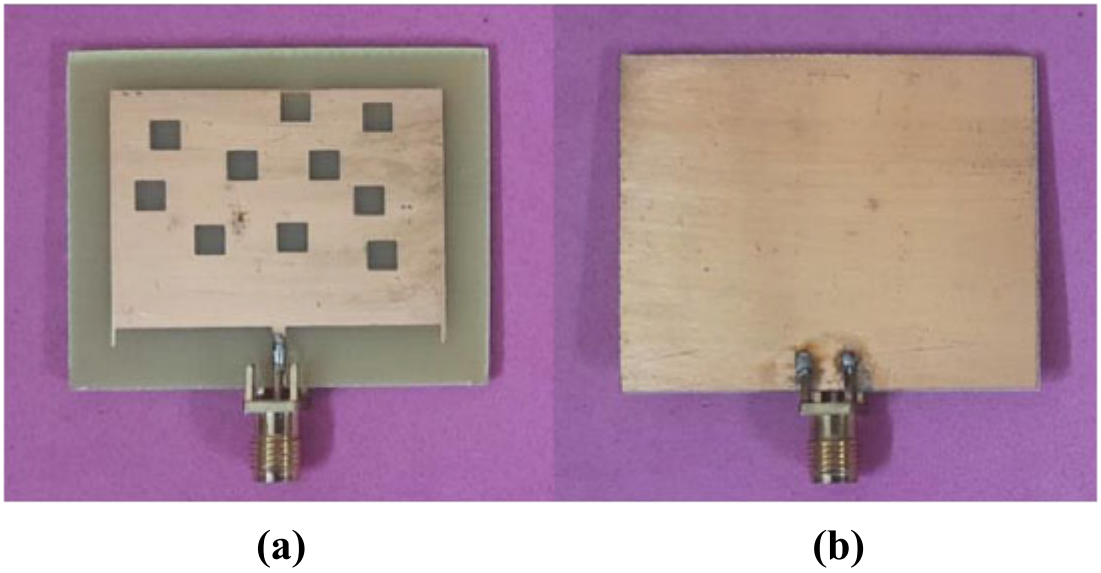

Fig. (2). Fabricated antenna (**a**) Front view (**b**) Back view.

For this article, the main contributions are as follows: (1) This paper presents a method for identifying bone fractures that involve a non-invasive approach. (2) A low-profile design for a 2.4 GHz antenna is created, simulated, and subjected to testing. (3) A bone phantom is both simulated and constructed to dielectric properties, and the analysis focuses on variations in the return loss. (4) The collected data is subjected to processing using DAS and DMAS beamforming algorithms for image reconstruction, with the microwave image unveiling the precise location of fractures.

2. MATERIALS AND METHODS

2.1. Antenna Measurement Results

The constructed antenna is investigated in terms of "Return loss, VSWR, Gain, Bandwidth, and Directivity" with the help of the VNA-Vector Network Analyzer. The simulation and the measured values are validated and analyzed. Because of transmission line imperfections, a few signals power is usually to source, when a signal is transferred on a transmission line. Return loss is an amount of this reflected power. A device is considered to be properly linked if return Loss is high. Because reflections impair the complete performance of the system, return loss ought to be less than -10dB [30]. Impedance matching is effective and provides lower insertion loss when the return loss is large [31]. A return loss of -45.24 dB is achieved at 2.4GHz in simulation, and -15.15 dB in testing, as depicted in Fig. (**3**). Thus, this antenna remains with a return loss below -10 dB, and it is ideal for real-time application.

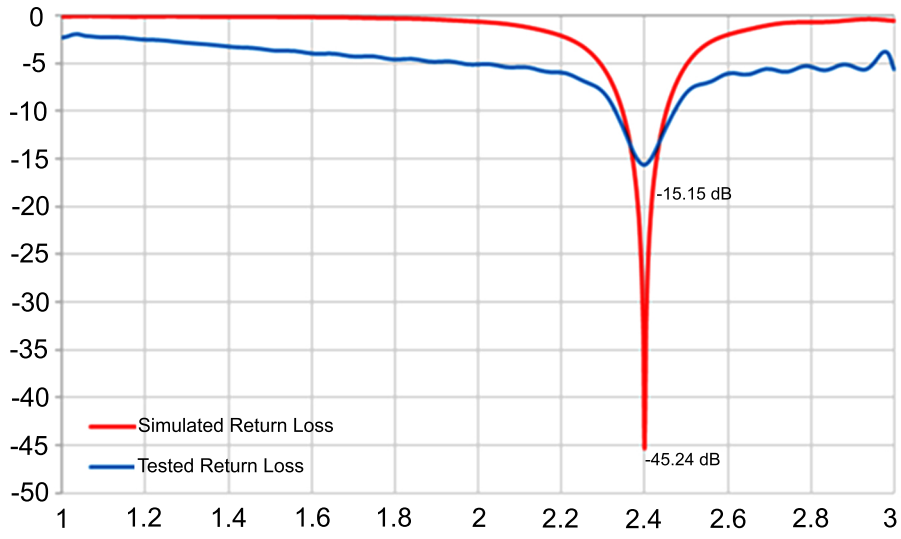

Fig. (3). Return loss comparison.

The VSWR is a measurement of the standing waves created in a feeder as a result of a mismatch, meanwhile, return loss is the quantity of power received by a load while power is given to it from a source. Another essential factor for the characteristics is the VSWR, which ought to have a value within 1 and 2 [32]. A simulated VSWR of 1.04 is attained at 2.4GHz, and 1.4 is attained while tested with VNA.

$$VSWR = \frac{1 + 10^{\frac{-RL}{20}}}{1 - 10^{\frac{-RL}{20}}} \quad \textbf{(1)}$$

The bandwidth is described as the band of frequencies over which it can work correctly [33]. At -10 dB, the absolute bandwidth across which the antenna satisfies is 105.3 MHz in simulation and 114.9 MHz in testing.

The proportion of radiated power in one direction to its power in isotropic direction is referred to as its gain [34]. It is recognized as the key parameter of an antenna since it pertains to the antenna system's efficiency. The directivity of an antenna is larger than its gain due to an efficiency factor known as "radiation efficiency".

$$G = K \times D \quad \textbf{(2)}$$

Where, G=gain, D=Directivity, and K=Antenna efficiency. Although losses are negligible in many antennas, the gain is approximately equivalent to the value of directivity. As a corollary, the terms gain and directivity are treated interchangeably. A gain and Directivity of 3.64dB and 4.1 dBi were attained at 2.4 GHz in simulation. Under testing, a gain of 2.87 dB is realized at 2.4GHz, as depicted in Fig. (**4**).

"Radiation pattern is described as a mathematical functional/graphical depiction of antenna's far field radiation qualities, as a function of EM wave's path of departure [35]. It is the term given to a plot of angle function in an antenna's field expression. It specifies the variability of an antenna's radiated power as a function of direction, away from the antenna". The designed antenna achieved the pattern of omnidirectional pattern as depicted in Fig. (**5**), which emits identical electromagnetic energy in all azimuthal directions, with energy increasing with elevation angle from the axis and decreasing to zero on the axis.

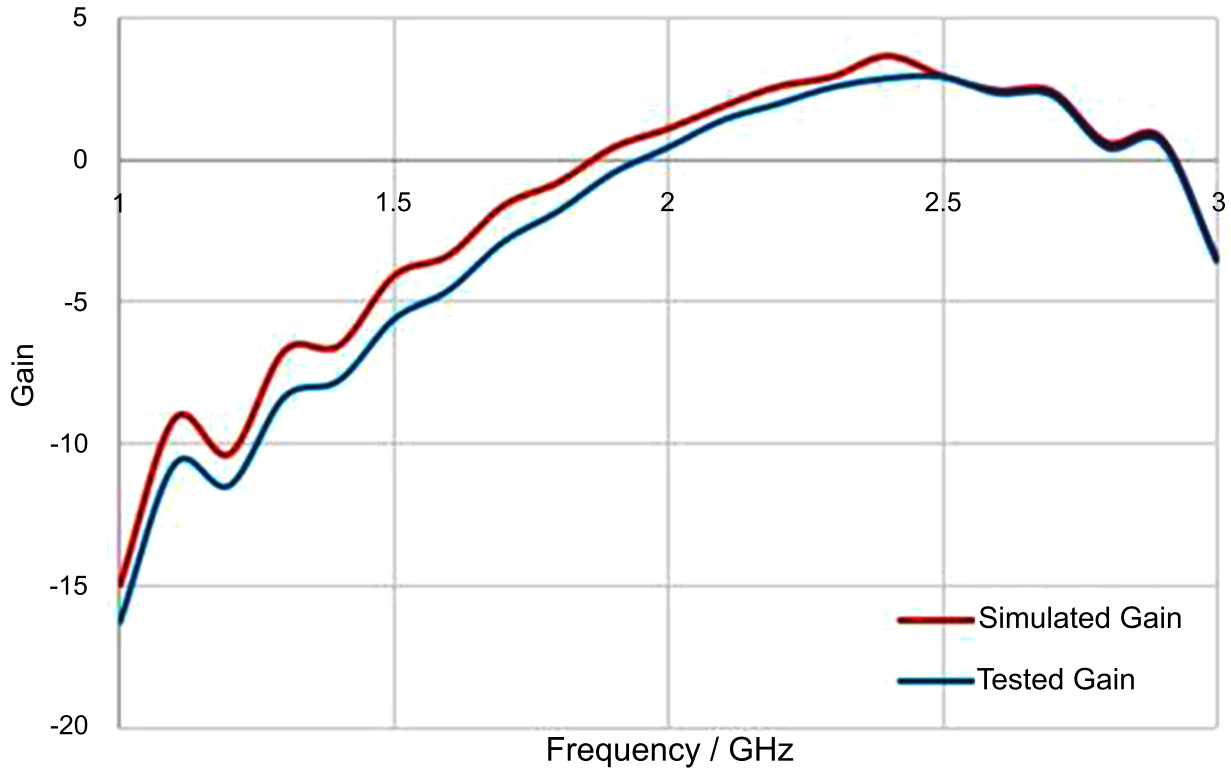

Fig. (4). Gain comparison.

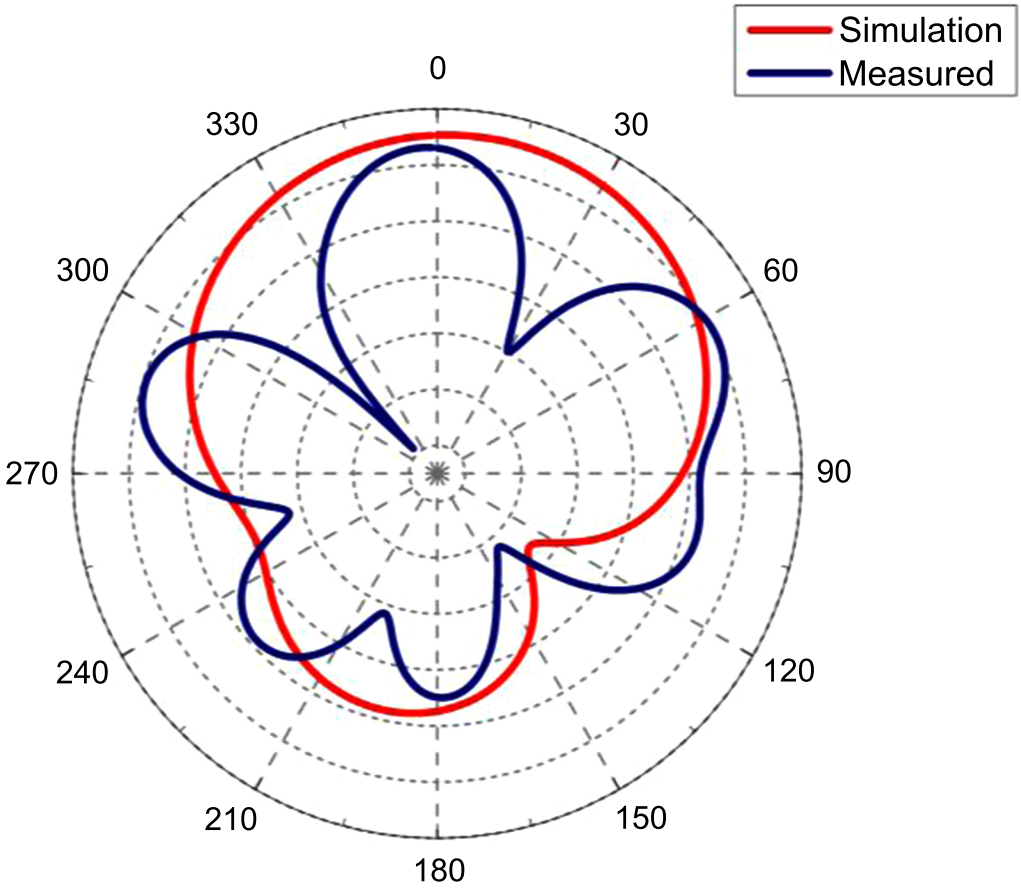

Fig. (5). Radiation pattern comparison.

Table 1. Antenna parameters.

Description	Simulated	Tested
Frequency	2.4 GHz	2.4 GHz
Return loss	-45.24 dB	-15.15 dB
VSWR	1.04	1.4
Bandwidth	105.3	114.9
Gain	3.64 dB	2.87
Radiation Pattern	Omnidirectional pattern	

Summarized simulated and tested antenna parameters are depicted in Table **1**.

3. BONE PHANTOM AND PROPAGATION ANALYSIS

The primary concept behind the research is to measure the return loss parameter in decibels for fracture detection. To test the antenna's functionality, the phantom muscle was constructed. The human arm is comprised of four sections. Skin, fat, muscle, and bone comprise the model. The deepest layer is bone, while the outer surface is skin. Between these two layers, muscle and fat are there. Bone was initially modeled by a uniform cylindrical shape with dielectric characteristics. This stage helped gather knowledge regarding fracture detection and identify crucial characteristics that hamper detection without effects that are confounded by geometry. Each layer has unique permittivity, conductivity, and density, as depicted in Table **2**. The predicted skin, fat, muscle, and bone dielectric constants are roughly 37, 5.3, 52, and 11.4, respectively. The skin, fat, muscle, and bone layers have thicknesses of 3, 7, 15, and 30 mm, correspondingly [36]. These measurements are generalizations and individual variations are little common among different people, but this remains the average value.

Table 2. Dielectric properties of bone.

Description	Permittivity	Electrical Conductivity	Density
Skin	37	0.148	1100
Fat	5.3	0.0776	1110
Muscle	52	0.461	1040
Bone	11.4	0.0063	1008

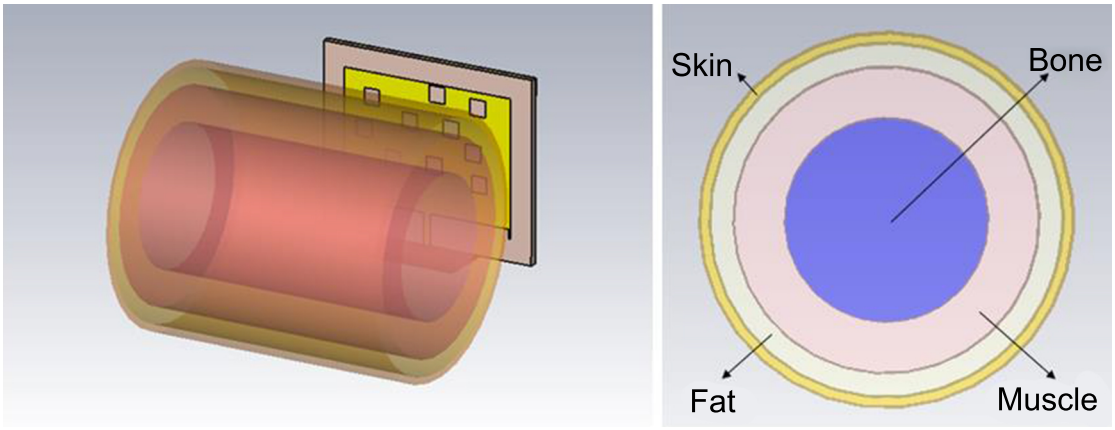

Fig. (6). Structure of bone phantom.

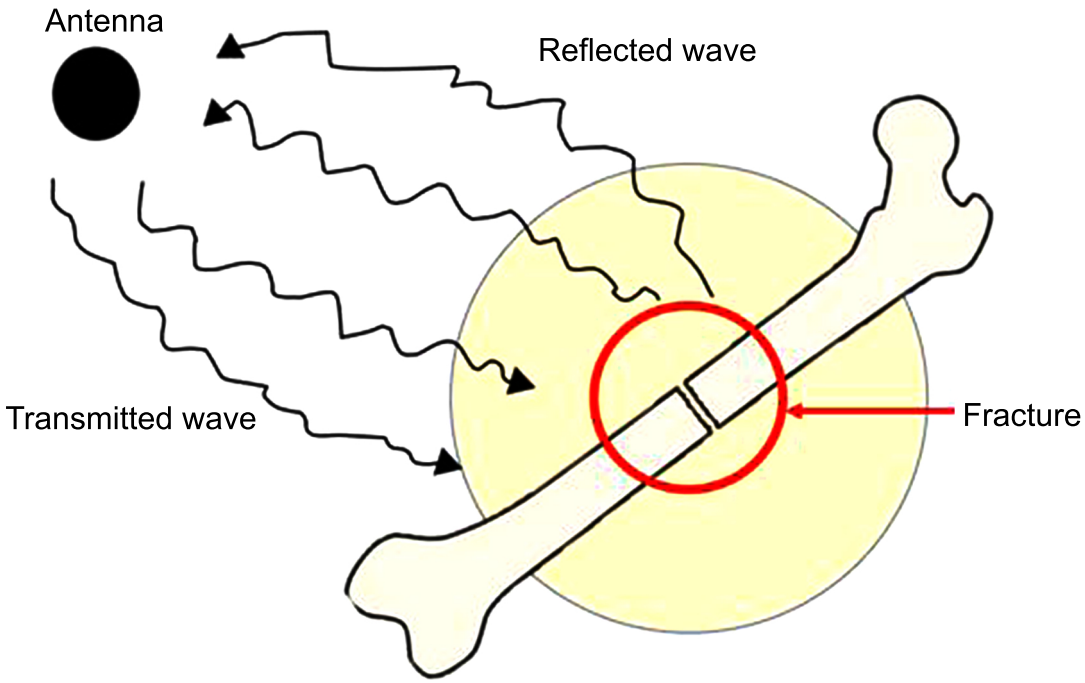

Fig. (7). Signal transmission for fracture detection.

The antenna is fitted to the arm design, to identify bone breaks, as depicted in Fig. (**6**). Human tissues' dielectric characteristics can serve as a reliable signal for diagnostic purposes [37]. The way electromagnetic (EM) waves interface with biological materials is governed by their dielectric characteristics, specifically their relative permittivity and conductivity [38]. The permittivity of the medium through which an electromagnetic wave passes determines its speed of propagation, and it interacts with the substance in three ways: absorption, reflections, and transmission. A substance's

dielectric characteristics might also be affected by elements, namely density, structural distortion, water content, porosity, *etc*. However, dielectric constant of bone depends on several factors, such as the frequency of electromagnetic waves, the orientation of the bone, and the presence of water and minerals in the bone. Generally, the dielectric constant of bone is higher at lower frequencies and decreases as the frequency increases. When a fracture occurs, the dielectric characteristics of the bone differ from healthy bone. The fracture can be recognized and found in the bone by monitoring these fluctuations. The dielectric disparity between healthy and fracture not only causes differences in reflection coefficients but how they assimilate incoming microwave radiation, as depicted in Fig. (**7**). The quantity of reflection is determined by the material's permittivity and frequency of the propagating signal. In the study that is being described, electromagnetic radiations are employed to assess the bone structure's dielectric characteristics without inflicting any damage. Cracks/fractures of varied lengths are generated in the bone model, and variations in the antenna's return loss are observed.

The screening for bone fracture *via* microwave imaging is based on substantial discrepancies in electromagnetic characteristics of normal and targeted anatomical objects/tissues. In quantified microwave imaging, the dielectric characteristics of biological tissues are rebuilt based on changes in complexity permittivity, as described by

$$\varepsilon^* = \varepsilon_r + j\frac{\sigma}{\omega\varepsilon_o} \quad (3)$$

Typically, due to an increase in frequency, conductivity rises, and permittivity falls. Debye's model is a mathematical model for parameterizing conductivity and permittivity levels with frequency dependency.

$$\varepsilon_r^* = \varepsilon_\infty + \frac{\varepsilon_s - \varepsilon_\infty}{1 - j\omega\tau} - \frac{j\sigma_o}{\omega\varepsilon_o} \quad (4)$$

$$\sigma^* = \sigma_\infty + \frac{\sigma_o - \sigma_\infty}{1 - j\omega\tau} \quad (5)$$

In terms of describing all dispersion difficulties, Debye's model has certain drawbacks. As a result, the Cole-Cole model was employed.

$$\varepsilon_r^* = \varepsilon_\infty + \frac{\varepsilon_s - \varepsilon_\infty}{1 - (j\omega\tau)^\alpha} - \frac{j\sigma_o}{\omega\varepsilon_o} \quad (6)$$

$$\sigma^* = \sigma_\infty + \frac{\sigma_o - \sigma_\infty}{1 - (j\omega\tau)^\alpha} \quad (7)$$

Where the factor is influenced by the substance's composition.

Since the human body is composed of several layers with varied conductivity and dielectric characteristics, whenever the antenna is operating nearer to the physical body, part of the radiated power is rivetted by the body, which leads to an increase in SAR value. The SAR is a critical measure for calculating the quantity of EM energy penetrated by bodily tissues [39]. W/kg is the usual unit for calculating SAR. SAR should be smaller than 1.6W/Kg, according to FCC rules [40]. The simulated SAR value of bone with an antenna is 1.25W/Kg, as depicted in Fig. (**8**).

$$SAR = \frac{\sigma |E|^2}{\rho} W/Kg \quad (8)$$

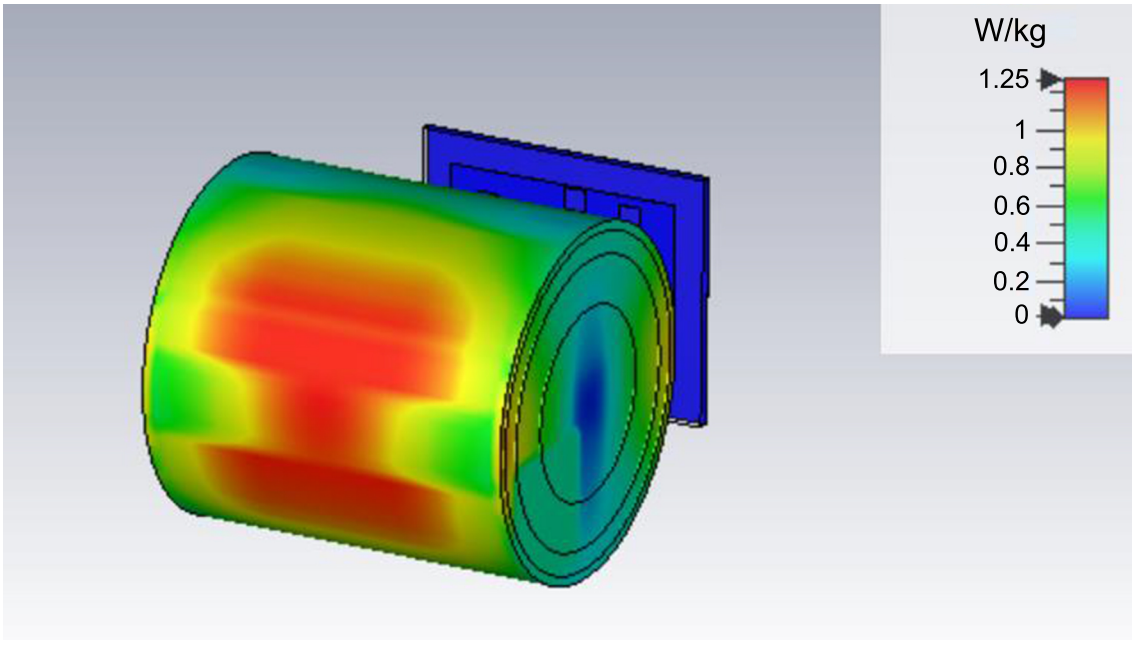

Fig. (8). SAR (simulated).

Time derivative of incremental energy-(dW), wasted in incremental mass-(dm), in an incrementally Volume-(dV), with a particular density-(ñ), is expressed as

$$SAR = \frac{d}{dt}\left(\frac{dW}{dm}\right) = \frac{d}{dt}\left(\frac{dW}{\rho(dV)}\right) \quad (9)$$

$$SAR = \frac{1}{\rho}\left(\frac{dW}{dt}\right) \quad (10)$$

Where dW implies absorbed energy, dm implies mass, and dV denotes volume. To calculate SAR, microwave waves of 1mW power are supplied to the antenna, and thermogram values are recorded prior to and following stimulation (20 minutes).

$$SAR = \frac{\Delta T}{\Delta t} C_t \, W/Kg \quad (11)$$

wherein T-temperature rise-(°C), t-time length for which microwave signals are administered-(second), and Ct-heat capacity-(J/kg/°C) of various tissues.

After 1200 seconds of excitement, the temperature climbed from 34.4°C to 34.8°C, and the 0.4°C increase stayed constant for an extended time frame. The antenna's SAR is therefore determined as 1.03 W/kg using expression (11).

Fig. (**9**) depicts a general perspective of the microwave imaging system developed and implemented in this study. The system is made up of a single antenna of the ISM band, which is linked to the VNA-Vector Network Analyzer. Coaxial cables were deployed to link VNA to an antenna. To prevent a mismatch between the VNA and cables, standard calibration was done after each channel at the start of each measurement step. Data have been collected between 1 to 3 GHz in frequency. Finally, the imaging technique is constructed using all of the signals that the VNA has received as input data.

Therefore, whenever antenna is put above the arm model, without crack/fracture, the reflection is exclusively owing to bone. If the bone has a crack (*i.e.*, the medium in a crack is air), return loss properties are controlled by bone's effective dielectric constant, and air gap. Return loss of -33.8 dB is attained, when the bone is simulated without crack. A partial slot is created with the air medium, as depicted in Fig. (**10a**), in their equivalent dielectric properties, and a return loss of -32.6 dB is obtained. Next, a full crack is made in the bone, as depicted in Fig. (**10b**), and a return loss of -31.5 dB is found. Fig. (**11**) depicts the graph of variation in terms of return loss under various scenarios of cracks in simulation is depicted in Table **3**.

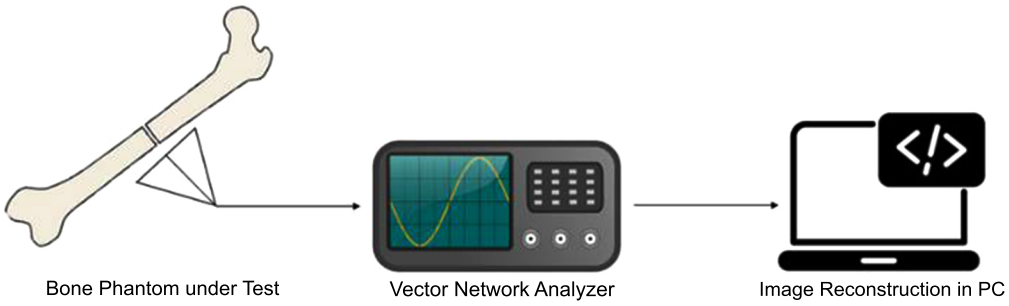

Fig. (9). Test setup of a functional prototype.

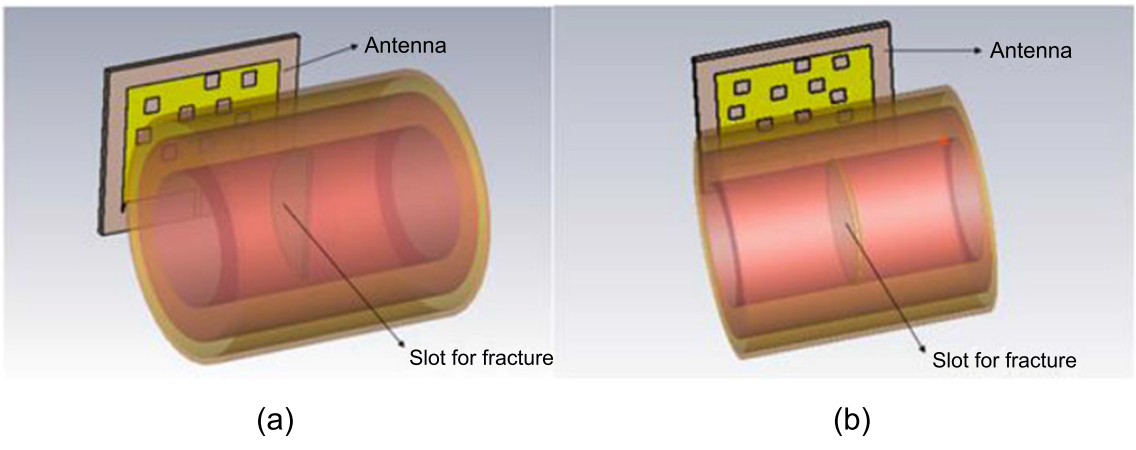

Fig. (10). (**a**) Bone with partial Slot, (**b**) Bone with full slot.

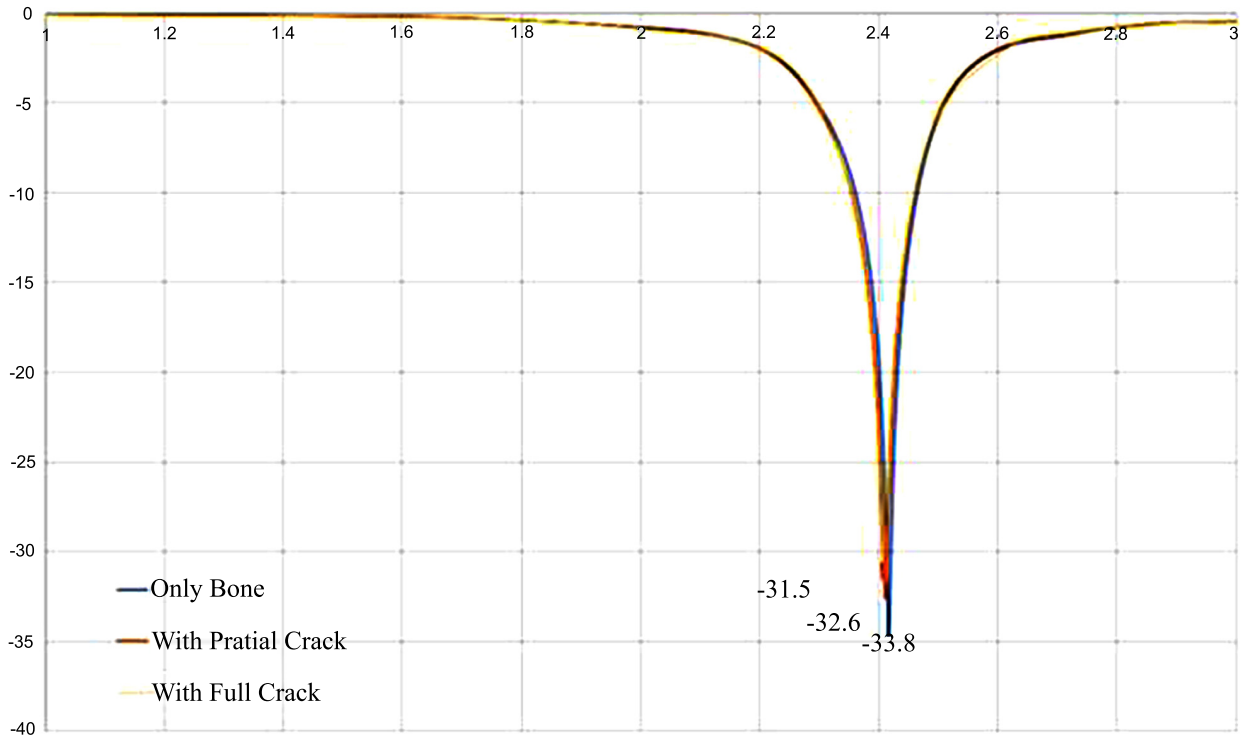

Fig. (11). Comparison of Return Loss (simulation).

Table 3. Return loss comparison (simulation).

Description	Return Loss (dB)
Only Bone	-33.8
With Partial Crack	-32.6
With Full Crack	-31.5

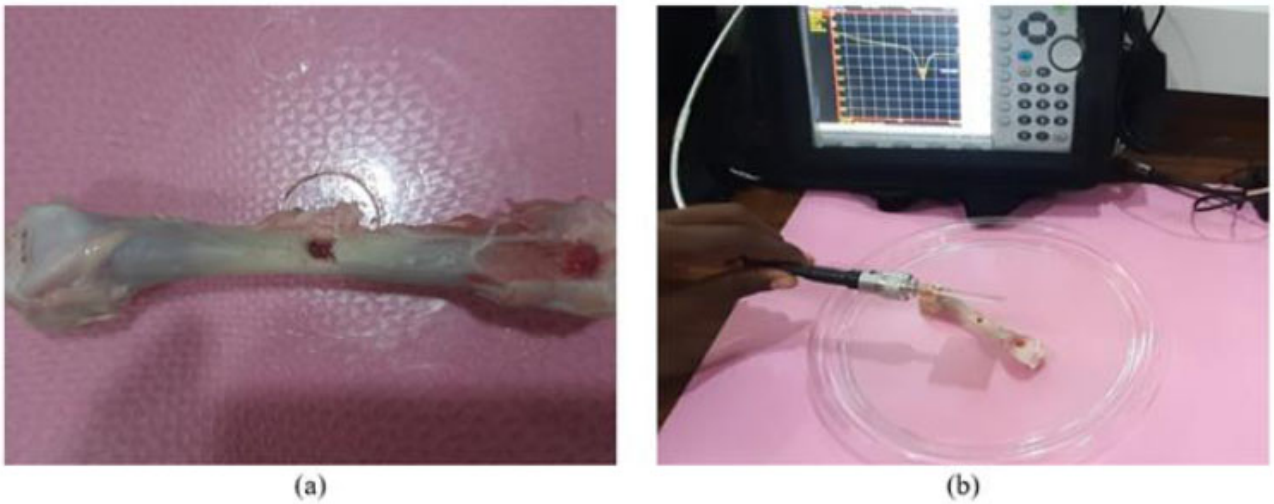

Fig. (12). (**a**) bone, (**b**) testing of antenna for fracture detection.

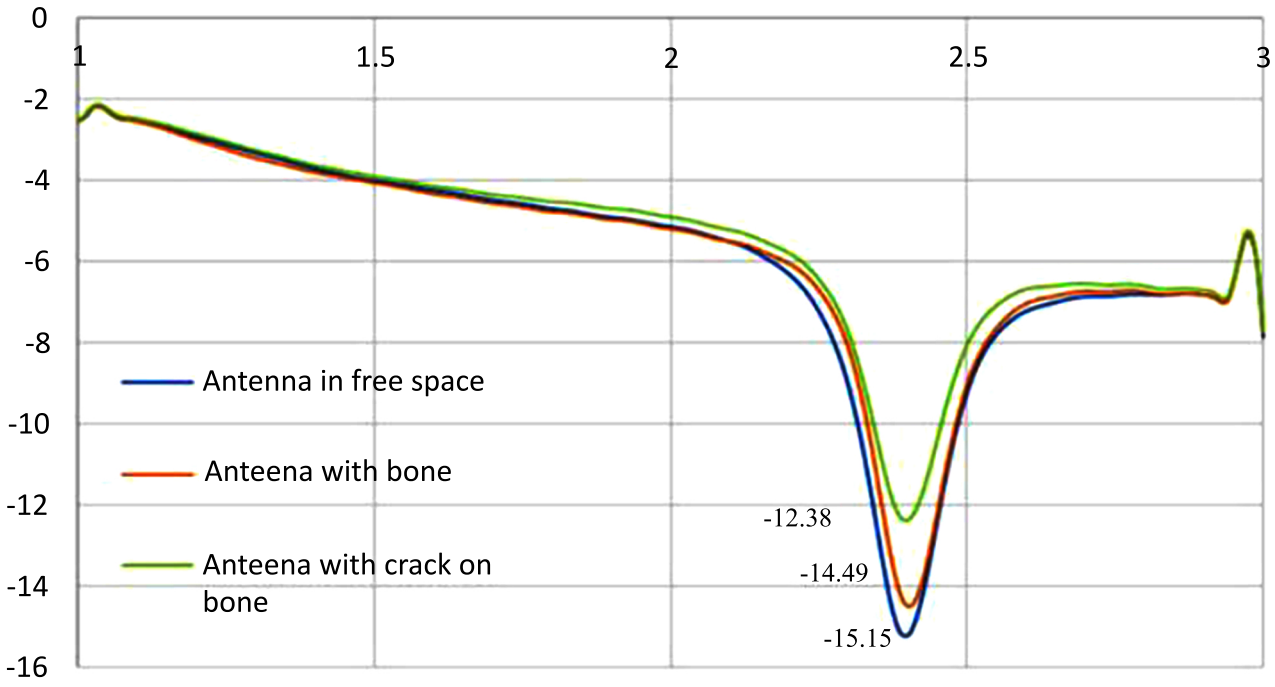

Fig. (13). Comparison of return loss.

Table 4. Return loss comparison (tested).

Description	Return Loss (dB)
In free space	-15.15
With bone	-14.47
With bone and crack	-12.38

Now, simulated findings were validated using chicken bone, as depicted in Fig. (**12**). The dielectric characteristics of the medium in the antenna change, when the fracture width was adjusted. As a response, there was a difference in return loss. This is the concept of detecting the cracks in the bone, for which an antenna is employed. When the antenna is suspended into free space, -15.15dB of return loss is attained. When the antenna is introduced near the bone, -14.47 dB is obtained. Next, a slot is introduced into the bone, and variations in the return loss are obtained. With a crack, -12.38 dB is obtained. The comparison of return loss of real-time testing is portrayed in the graph in Fig. (**13**) and Table **4**.

The antenna has been designed, as well as, fabricated, and their parameters are analysed. Further, a bone phantom is designed with their equivalent dielectric constants and the return loss with bone and with cracks are analyzed. Thus, this gives a satisfactory performance, in terms of the return loss, for image reconstruction.

4. RESULTS AND DISCUSSION

4.1. Image Reconstruction

An enduring and popular method for biomedical diagnostics to locate a tumor or other abnormalities in the human body is medical imaging. Radiation exposure and healthcare expenses are now being raised by the overuse of particular imaging technologies [41]. Due to excessive radiation exposure, radiation from traditional medical imaging systems has emerged as a serious health hazard [42]. The overabundance of imaging-based medical diagnostics has expanded exposure to ionizing radiation and raised concerns about unintended impacts on human health [43]. The negative effects on the human body, and reliability concerns brought up by traditional imaging technologies are now actively considered.

Microwave imaging is a useful diagnostic technique for non-invasively visualizing the dielectric characteristics of non-metallic things. Microwaves are increasingly being used for imaging soft tissues in biological applications due to significant differences in their dielectric characteristics. It has recently been discovered that the dielectric characteristics of diseased or malignant tissues differ significantly from those of healthy tissues. This concept has been investigated in a bid to spot the fracture. Because the photon energy of a microwave is reasonably low, it is regarded to be safer than X-rays. Nonetheless, to properly investigate this study topic, the dielectric characteristics of a variety of biological tissues (both healthy and malignant) must first be correctly established to differentiate dielectric properties between diverse types of tissues.

The majority of commercially available ultrasound medical imaging devices use conventional "Delay and Sum-(DAS)" beamforming to provide B-mode pictures. The "delay and sum" algorithm is a beamforming technique used to combine signals received from an array of transducers or antennas to enhance resolution and Signal-to-Noise Ratio of final output signal. The basic idea behind this algorithm is to introduce a time delay to the signals received by each element in the array and then add the delayed signals to generate a beamformed signal. By modifying their time delays following the separation of the source and detectors, the DAS adds the necessary US signals [44]. Basic theory for the standard DAS beamformer is

$$I(\vec{r}) = \sum_{M}^{i=1} b_i(\tau_i(\vec{r}))^2 \quad \textbf{(12)}$$

wherein b_i is indeed the backscattered signal captured at Channel *i*, M represents the entire channel number, and $\tau_i(\vec{r})$ is the amount of time needed to transmit the entire range between the antenna (*i*) and the focal point $r^{\rightarrow} = (x, y, z)$.

The signal generated at multiple paths is initially time-oriented, with each focus point $r^{\rightarrow}$. Calculating the time delay for every single backscattered signal is a step in the time procedure. The anticipated average bone propagation speed and round-trip distance between the focus point $\tau_i(\vec{r})$, and antenna were deployed to estimate the delay for each signal, intercepted at the antenna. Time-aligned signals are then simply added afterward. It is predicted that any fracture-related reflections will accumulate coherently. On the other hand, it is anticipated that reflections from healthy tissues and any pre-processing artifacts may combine incoherently. A bone picture is constructed by allocating the energies of the cumulative signal, which is frequently estimated across a time frame, to the intensity of each focus point inside the volume of the bone.

Delay-and-sum algorithm can be used for processing signals from a single antenna in various applications. In a single-antenna delay and sum algorithm, the received signal is first split into multiple channels, each with a different time delay. The time delay is adjusted based on the expected location and direction of the target signal. Then, the delayed signals from each channel are summed to form a beamformed signal. The algorithm for the DAS beamforming is mentioned below.

Algorithm 1 Delay-and-Sum (DAS) Algorithm

```
procedure DAS(received_data, delays, speed_of_sound, sampling_rate)
    width ← size(received_data, 1)
    height ← size(received_data, 2)
    num_elements_x ← size(received_data, 3)
    num_elements_y ← size(received_data, 4)
    reconstructed_image ← zeros(width, height)
    for x ← 1 to width do
        for y ← 1 to height do
            pixel_sum ← 0
            for i ← 1 to num_elements_x do
                for j ← 1 to num_elements_y do
                    delay ← delays(x, y, i, j)
                    delayed_index ← round(delay × sampling_rate)
                    pixel_sum ← pixel_sum + received_data(i, j, delayed_index)
                end for
            end for
            reconstructed_image(x, y) ← pixel_sum
        end for
    end for
    return reconstructed_image
end procedure
```

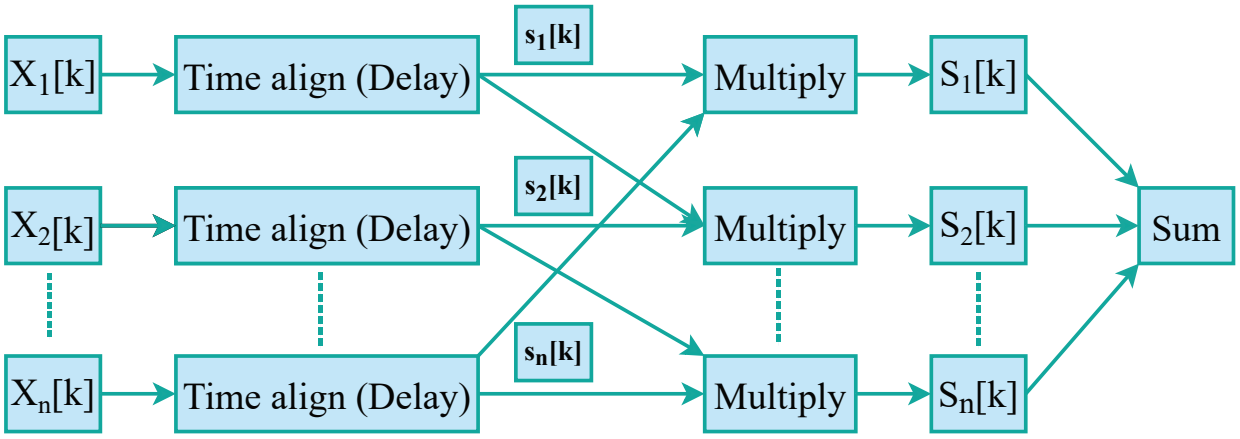

Fig. (14). DMAS algorithm.

Nevertheless, the aperture size and operation frequency have an impact on the picture quality and contrast that may be achieved with DAS [45]. With greater contrast, more pronounced main lobes, and feeble side lobes than DAS, DMAS offers improved image quality [46]. With an extra multiplication stage, the "DMAS" beamformer is comparable to traditional DAS. Yet, contrasted to DAS, DMAS is anticipated to offer improved clutter reduction since it substantially increases sample size, by Signal-pair multiplication.

The "delay-multiply-and-sum (DMAS)" algorithm is a beamforming strategy employed in medical ultrasound imaging to generate images from the echoes acknowledged by a transducer. DMAS algorithm is based on the principle of spatial coherence of the echoes, meaning that echoes from the same point in space will be highly correlated.

Generally, DMAS method is applied for array of transducer elements in medical imaging. However, it is possible to adapt the DMAS algorithm for use with a single transducer element. In a single-element DMAS algorithm, the beamforming process is achieved by changing the time delay of the received signal rather than by delaying and summing signals received by multiple elements. Time delay is adjusted based on the assumed position of the reflecting object, and the beamforming is achieved by multiplying and summing the delayed signals and the process is depicted in Fig. (**14**).

First, the signal is reflected, dispersed, and transmitted in response to the dielectric properties of bone. Received backscattered signal is pre-processed before being used to determine the focal point. The acknowledged signal is first time-shifted, then multiplied in sets, and then added to generate the focal point. The antenna detects the signal reflected by the bone. The location of the fracture can be determined by scanning the bone in a planar fashion and gathering backscattered signal S11(dB), at individual scan points. Time delays are calculated by converting the round-trip route length between the antennas. Using the time delays as a foundation, the resultant signal is time-shifted. The delay is replaced by phase shifting, and the multiplication is replaced by complex conjugation. The phase shift is based on the assumed angle of incidence of the echo at the antenna, and the complex conjugation is used to account for the difference in polarity between the transmitted and received signals. The intensity of the focal point is obtained by integrating over a time interval. The above technique is performed for each focal point in the bone region. On every focus point, the DMAS algorithm conducts a correlation process to produce highly comparable data. The significant increase in sample quantity is what has enabled the accuracy of the generated images to improve. With delay values derived as follows, the findings are moved by focal points in the imaging domain.

The average of backscattered signals received at multiple locations is employed in the mean value process. If the reflection coefficient approaches zero, the bone gets more power; nevertheless, the null reflection displays a negative infinity value. When the antenna is perfectly positioned on the fracture, it will reflect more power and have a higher mean value. As a result, the mean value of the reflected signal is higher near the center, *i.e.*, fracture, than at the edge due to the bone structure.

$$I_{DMAS} = \sum_{K=1}^{L} \left(\sum_{i=1}^{M} \sum_{j=1}^{M} S_i[k]\, S_j[k] \right) \quad \textbf{(13)}$$

Where, M represents the overall number of signals received, $S_i[k]$ and $S_j[k]$ are delayed signals, based on the locations of transmitter, and reception antennas, and M is a weighted sum of signals received. As a result, the difference in mean value with, and without the fracture is computed to determine the fracture site. The DMAS beamforming algorithm reforms the picture of the bone. The technique is well-suited to producing high-resolution pictures and detecting bone fractures. The algorithm for the DMAS beamforming is mentioned below.

Because of the great intensity of the image, the specific position of the fracture is evident. The clear image of the fracture may be seen in the photograph's center at the highest yellow hue pixel value. The bone's greatest reflection causes

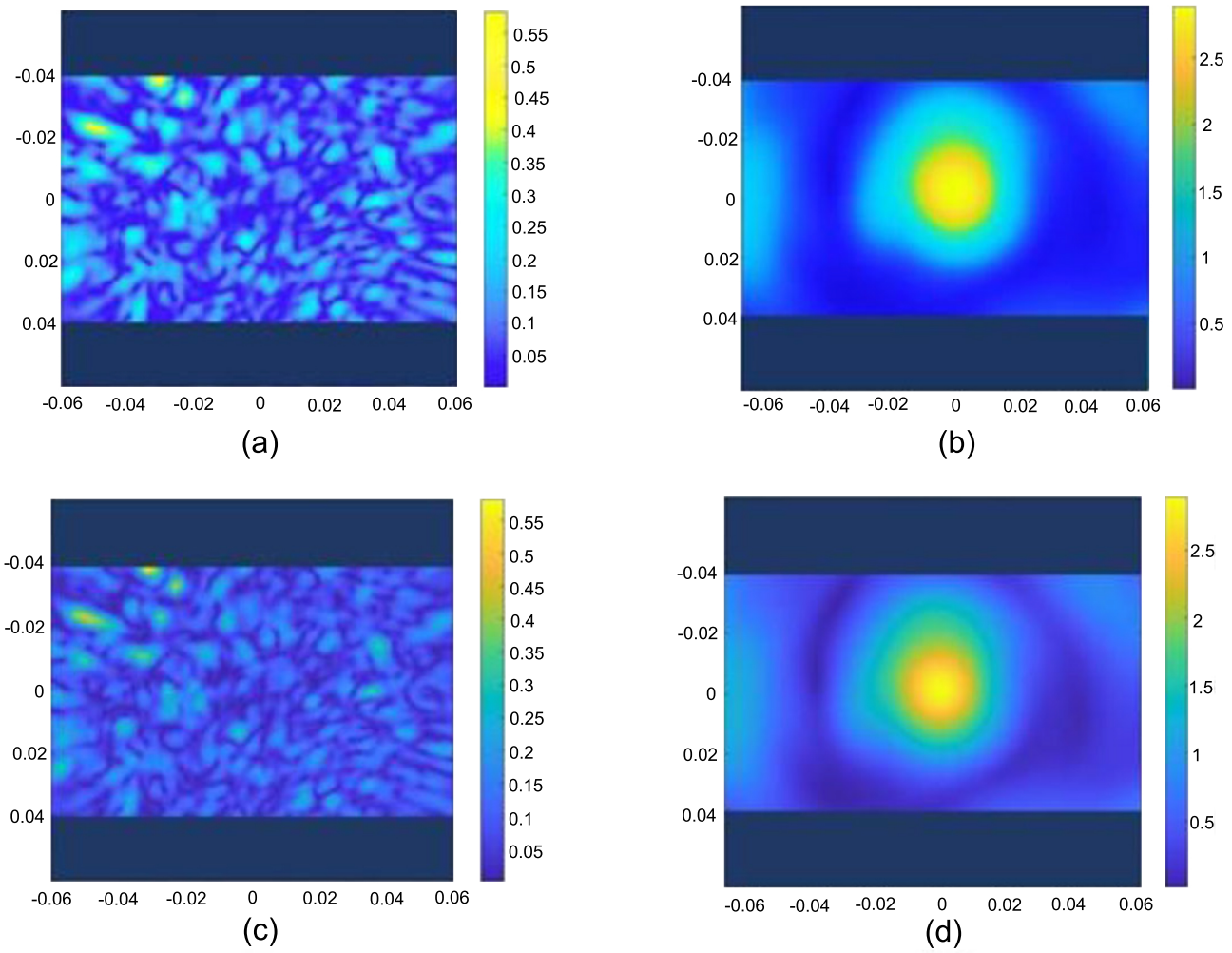

Fig. (15). Reconstructed image (**a**) Bone without crack-DAS (**b**) Bone with crack-DAS (**c**) Bone without crack-DMAS (**d**) Bone without crack-DMAS.

the image's richest golden brilliance. The intensity of the remaining blue and pale-yellow colors is the lowest, expanding outward from the bone.

DMAS effectively elevates both contrast and resolution compared to the delay and sum (DAS) beamforming technique. Therefore, DMAS has overcome its inherent shortcomings, including low picture resolution and apparent off-axis clutter. Visual investigations imply that DMAS beamforming simply often has a lesser background noise level than those with DAS beamforming because the background area of the DMAS image seems to be darker than the DAS image, as depicted in Fig. (**15**). DMAS can provide better resolution and contrast in the resulting image by emphasizing the signals that are in-phase and suppressing the out-of-phase signals. Furthermore, the DMAS algorithm can effectively recognize many targets. For situations with poor picture contrasts and resolution, the DMAS method may hold great promise.

CONCLUSION

This research shows a novel design and performance investigation of a 2.4 GHz ISM band antenna for fracture detection. This research is focused on the evaluation of return loss as it varies depending on the state of the bone fracture. The proposed antenna is put above the arm model in simulation, and variations in return loss characteristics are investigated. The designed and fabricated antenna shows satisfactory performance in terms of return loss variation once it is placed on the arm model and for the various types of bone cracks in both simulation and the real-time testing of phantom. The data gathered are processed with DAS beamforming and DMAS beamforming for the image reconstruction. To view a 2D picture of the scanned region and identify the bone fracture, these signals are then converted to digital data and analyzed. Comparing the reconstructed pictures leads to the conclusion that although DMAS accurately identifies the position and size of the bone fracture, the DAS algorithm just offers a hint about the fracture's presence. Based on the data inferred, intensity and resolution are considerably improved by DMAS contrasted to the delay and sum (DAS) beamforming method. Thus, DMAS beamforming offers a superior quality of images than DAS beamforming.

The comparison between the proposed and the SOTA is as follows: Numerous scholars have suggested a range of approaches to monitor across different frequency levels, encompassing the creation of a small-sized microwave tool

specifically intended for detecting fractures. The mentioned sensor in a study [16], functioning at 2.45 GHz, faces obstacles such as the loss of high-frequency components during the process of image restoration, resulting in a blurred final image. The antenna [17] lacks a low-profile design, and a suitable detection system is deficient for reconstructing images. A study [18] states a planar monopole antenna, where the difficulty with this system arises from its considerable size of the system. A smart bone plate was introduced [19] which employs electrical impedance spectroscopy to track tissue healing. Nevertheless, this system is constrained by its reliance on impedance variation, introducing limitations to its application. Thus, an enhanced version of the patch antenna is proposed here, which gives significantly better results than the existing design. In this design, a miniaturized version of the patch antenna is designed in a lower frequency band for the deeper penetration of EM waves into the body tissues, and the signal losses can be avoided. A Low-profile antenna is suggested, and it offers a compact size for easy integration and portability, with advantages in reduced interference, improved aesthetics, and enhanced safety in diverse applications. And no initial tuning of the system is required since all parameters are predefined.

Another comparison is between the algorithms employed for the image reconstruction. The GPR algorithms in a study [22] present challenges in computational complexity, potential trade-offs between accuracy and resolution, sensitivity to subsurface properties, limitations in penetrating certain materials, susceptibility to noise, and difficulties in heterogeneous subsurface conditions. While the DGCA method in a study [23] shows promise in improving high-resolution image inpainting, its complexity, involving a two-stage network with parallel structures and contextual attention modules, might pose challenges in terms of computational efficiency. One potential disadvantage of the proposed image restoration method [24], which combines Semantic Priors and Deep Attention Residual Group, maybe its computational complexity. The incorporation of multiple components, including Semantic Priors Network, Deep Attention Residual Group, and Full-scale Skip Connection, could lead to increased processing requirements. This complexity may affect the method's efficiency, especially in real-time applications. However, Delay-and-Sum (DAS) offers simplicity and real-time processing advantages in the context of beamforming. DAS enhances the signal from the desired direction while attenuating signals from other directions. The simplicity of DAS makes it easy to implement, and its suitability for real-time processing applications adds to its appeal. Delay-Multiple-and-Sum (DMAS) represents an advancement over DAS by introducing multiple delays to each signal before summation. This modification enhances the performance of the beamforming process, especially in scenarios with complex interference or multipath propagation. DMAS provides improved adaptability to varying environmental conditions, making it a suitable choice for applications where higher performance is essential. In this study both DAS and DMAS have been implemented, where the DMAS offers an excellent performance, improved image quality, and simplicity of the algorithm and yet is effective. The outcomes indicate that the suggested approach outperforms existing SOTA methods. The results attested to the approach's potential for improving bone fracture identification, which is cost-efficient, reliable, and yet effective detection.

While microwaves can penetrate certain materials well, they may face challenges when imaging through highly absorbing or dense materials. The penetration depth is influenced by factors such as frequency and material properties. This can be overcome by using an antenna design with a lower frequency band, using low dielectric constant substrate material, larger and thinner patches, and proper impedance matching. Achieving high contrast resolution in microwave imaging can be challenging, particularly when distinguishing between tissues with similar dielectric properties. Implementing a good-performance antenna with beamforming techniques and polarization control improves the resolution of the image, based on hardware. On software, Synthetic aperture radar (SAR) processing, inverse scattering techniques, adaptive filtering, and image fusion can improve the quality of microwave images, further leading to an enhanced version of this study.

LIST OF ABBREVIATIONS

VSWR	=	Voltage Standing Wave Ratio
FCC	=	Federal Communication Commission
ISM	=	Industrial Scientific Medical
SAR	=	Specific Absorption Rate
DMAS	=	Delay-Multiply-and-Sum
DAS	=	Delay-and-Sum

ETHICS APPROVAL AND CONSENT TO PARTICIPATE

Not applicable.

HUMAN AND ANIMAL RIGHTS

No animals/humans were used for studies that are the basis of this research.

CONSENT FOR PUBLICATION

Not applicable

AVAILABILITY OF DATA AND MATERIALS

Not applicable.

FUNDING

No funding to declare.

CONFLICT OF INTEREST

The authors declare no conflict of interest.

ACKNOWLEDGMENTS

Declared none.

REFERENCES

[1] Yadav DP, Rathor S. Bone fracture detection and classification using deep learning approach. 2020 International Conference on Power

Electronics & IoT Applications in Renewable Energy and its Control (PARC). 28-29 February 2020; Mathura, India. 2020. [http://dx.doi.org/10.1109/PARC49193.2020.236611]

[2] Karimunnisa S, Savarapu PR, Madupu RK, Basha CZ, Neelakanteswara P. Detection of bone fractures automatically with enhanced performance with better combination of filtering and neural networks. 2020 Second International Conference on Inventive Research in Computing Applications (ICIRCA). Coimbatore, India. 2020; pp. 189-93. [http://dx.doi.org/10.1109/ICIRCA48905.2020.9183085]

[3] Kenwright J, Richardson JB, Cunningham JL, *et al.* Axial movement and tibial fractures. A controlled randomised trial of treatment. J Bone Joint Surg Br 1991; 73-B(4): 654-9. [http://dx.doi.org/10.1302/0301-620X.73B4.2071654] [PMID: 2071654]

[4] Pham DL. Two-photon excitation fluorescence microscopy. Annu Rev Biomed Eng 2000; 2: 399-429. [http://dx.doi.org/10.1146/annurev.bioeng.2.1.315]

[5] Nahid AA, Khan TM, Kong Y. Hardware implementation of bone fracture detector using fuzzy method along with local normalization technique. Annals of Data Science 2017; 4(4): 533-46. [http://dx.doi.org/10.1007/s40745-017-0118-z]

[6] Mercuri M, Sheth T, Natarajan MK. Radiation exposure from medical imaging: A silent harm? CMAJ 2011; 183(4): 413-4. [http://dx.doi.org/10.1503/cmaj.101885] [PMID: 21324851]

[7] Nathanael EJ, Wyawahare MV. Survey of bone fracture detection techniques. Int J Comput Appl 2013; 71(17): 31-4. [http://dx.doi.org/10.5120/12452-9342]

[8] Matsuda M. High-dose proton beam therapy *versus* conventional fractionated radiation therapy for newly diagnosed glioblastoma: A propensity score matching analysis. Radiat Oncol 2023; 18: 138. [http://dx.doi.org/10.1186/s13014-023-02236-1]

[9] Griffet J, Leroux J, Boudjouraf N, Abou-Daher A, el Hayek T, Karunanithi S. Elastic stable intramedullary nailing of tibial shaft fractures in children. J Child Orthop 2011; 5(4): 297-304. [http://dx.doi.org/10.1007/s11832-011-0343-5]

[10] Larsen LE, Jacobi JH. Microwave scattering parameter imagery of an isolated canine kidney. Med Phys 1979; 6(5): 394-403. [http://dx.doi.org/10.1118/1.594595] [PMID: 492073]

[11] Lazebnik M. A large-scale study of the ultrawideband microwave dielectric properties of normal, benign and malignant breast tissues obtained from cancer surgeries. Phys Med Biol 2007; 52(20): 6093-115. [http://dx.doi.org/10.1088/0031-9155/52/20/002]

[12] Qaddoumi N, El-hag AH, Al Hosani M, Mansouri IA, Ghufli HA. Detecting defects in outdoor non-ceramic insulators using near-field microwave non-destructive testing. IEEE Trans Dielectr Electr Insul 2010; 17(2): 402-7. [http://dx.doi.org/10.1109/TDEI.2010.5448094]

[13] Zarifi MH, Deif S, Abdolrazzaghi M, *et al.* A microwave ring resonator sensor for early detection of breaches in pipeline coatings. IEEE Trans Ind Electron 2018; 65(2): 1626-35. [http://dx.doi.org/10.1109/TIE.2017.2733449]

[14] Subbaraj S, Ramalingam VS, Kanagasabai M, Sundarsingh EF, Selvam YP, Kingsley S. Electromagnetic nondestructive material characterization of dielectrics using ebg based planar transmission line sensor. IEEE Sens J 2016; 16(19): 7081-7. [http://dx.doi.org/10.1109/JSEN.2016.2591320]

[15] Staderini EM. UWB radars in medicine. IEEE Aerosp Electron Syst Mag 2002; 17(1): 13-8. [http://dx.doi.org/10.1109/62.978359]

[16] Ramalingam S, Kanagasabai M, Sundarsingh EF. A compact microwave device for fracture diagnosis of the human tibia. IEEE Trans Compon Packag Manuf Technol 2019; 9(4): 661-8.

[17] Lin X, Chen Y, Gong Z, Seet B, Huang L, Lu Y. Ultrawideband textile antenna for wearable microwave medical imaging applications. IEEE Trans Antennas Propag 2020; 68(6): 4238-49. [http://dx.doi.org/10.1109/TAP.2020.2970072]

[18] Boologam AV, Krishnan K, Palaniswamy SK, *et al.* Onthe design and development of planar monopole antenna forbone crack/void detection. Int J Antennas Propag 2022; 2022: 1-12. [http://dx.doi.org/10.1155/2022/4663488]

[19] Lin MC, Hu D, Marmor M, Herfat ST, Bahney CS, Maharbiz MM. Smart bone plates can monitor fracture healing. Sci Rep 2019; 9(1): 2122. [http://dx.doi.org/10.1038/s41598-018-37784-0] [PMID: 30765721]

[20] Ruvio G, Cuccaro A, Solimene R, Brancaccio A, Basile B, Ammann MJ. Microwave bone imaging: A preliminary scanning system for proof□of□concept. Healthc Technol Lett 2016; 3(3): 218-21. [http://dx.doi.org/10.1049/htl.2016.0003] [PMID: 27733930]

[21] Khalesi B, Sohani B, Ghavami N, Ghavami M, Dudley S, Tiberi G. A phantom investigation to quantify huygens principle based microwave imaging for bone lesion detection. Electronics 2019; 8(12): 1505. [http://dx.doi.org/10.3390/electronics8121505]

[22] Lalitha K, Manjula J. Non-invasive microwave head imaging to detect tumors and to estimate their size and location. Phys Med 2022; 13: 100047. [http://dx.doi.org/10.1016/j.phmed.2022.100047]

[23] Chen Y, Xia R, Yang K, Zou K. DGCA: high resolution image inpainting *via* DR-GAN and contextual attention. Multimedia Tools Appl 2023; 82(30): 47751-71. [http://dx.doi.org/10.1007/s11042-023-15313-0]

[24] Chen Y, Xia R, Yang K, Zou K. DARGS: Image inpainting algorithm *via* deep attention residuals group and semantics. Journal of King Saud University - Computer and Information Sciences 2023; 35(6): 101567. [http://dx.doi.org/10.1016/j.jksuci.2023.101567]

[25] Adegoke M. Design of multiband microstrip antenna for mobile wireless communication. Proceedings of the 2015 International Conference on Management, Education, Information and Control. [http://dx.doi.org/10.2991/meici-15.2015.29]

[26] Asokan V, Thilagam S, Kumar KV. Design and analysis of microstrip patch antenna for 2.4GHz ISM band and WLAN application. 2015 2nd International Conference on Electronics and Communication Systems (ICECS). 26-27 February 2015; Coimbatore, India. 2015. [http://dx.doi.org/10.1109/ECS.2015.7124756]

[27] Karthick M. Design of 2.4GHz patch antennae for WLAN applications. 2015 IEEE Seventh National Conference on Computing, Communication and Information Systems (NCCCIS). 1-4. [http://dx.doi.org/10.1109/NCCCIS.2015.7295902]

[28] Damaj AW, El Misilmani HM, Chahine SA. Implantable antennas for biomedical applications: An overview on alternative antenna design methods and challenges. 2018 International Conference on High Performance Computing & Simulation (HPCS). Orleans, France. 2018; pp. 31-7. [http://dx.doi.org/10.1109/HPCS.2018.00019]

[29] Sheela JJJ, Logeshwaran M, Kumar KU, Vamsi M, Kumar NC. Design of ultra-wideband of rectangular shaped emoji designed microstrip patch antenna of 4.5GHz for military applications. 2022 3rd International Conference on Smart Electronics and Communication (ICOSEC). 20-22 October 2022; Trichy, India. 2022. [http://dx.doi.org/10.1109/ICOSEC54921.2022.9951893]

[30] Faisal M, Gafur A, Rashid SZ, Shawon MO, Hasan KI, Billah MB. Return loss and gain improvement for 5G wireless communication based on single band microstrip square patch antenna. 2019 1st International Conference on Advances in Science, Engineering and Robotics Technology (ICASERT). 03-05 May 2019; Dhaka, Bangladesh. 2019. [http://dx.doi.org/10.1109/ICASERT.2019.8934474]

[31] Upadhyay D, Dwivedi RP. Antenna miniaturization techniques for wireless applications. 2014 Eleventh International Conference on Wireless and Optical Communications Networks (WOCN). Vijayawada, India. 2014; pp. 1-4. [http://dx.doi.org/10.1109/WOCN.2014.6923083]

[32] Jyosthna R, Sunny RA, Jugale AA, Ahmed MR. Microstrip patch antenna design for space applications. 2020 International Conference on Communication and Signal Processing (ICCSP). Chennai, India. 2020; pp. 406-10. [http://dx.doi.org/10.1109/ICCSP48568.2020.9182250]

[33] Mohamed Junaid KA, Sheela JJJ, Logeshwaran M. Design and analysis of novel face shaped microstrip array antenna of UWB for early breast tumor detection. 2022 Sixth International Conference on I-SMAC (IoT in Social, Mobile, Analytics and Cloud) (I-SMAC). [http://dx.doi.org/10.1109/I-SMAC55078.2022.9987380]

[34] Moore R. Effects of a surrounding conducting medium on antenna analysis. IRE Trans Antennas Propag 1963; 11(3): 216-25. [http://dx.doi.org/10.1109/TAP.1963.1138043]

[35] Simanjuntak AB. Preliminary design of automatic antenna radiation pattern measurement system for antenna and propagation laboratory course. Proceedings of the 5th UPI International Conference on Technical and Vocational Education and Training (ICTVET 2018). [http://dx.doi.org/10.2991/ictvet-18.2019.19]

[36] Ullah M, Islam M, Alam T, Ashraf F. Paper-based flexible antenna for wearable telemedicine applications at 2.4 GHz ISM band. Sensors 2018; 18(12): 4214.

[http://dx.doi.org/10.3390/s18124214] [PMID: 30513719]

[37] Joines WT, Jirtle RL, Rafal MD, Schaefer DJ. Microwave power absorption differences between normal and malignant tissue. Int J Radiat Oncol Biol Phys 1980; 6(6): 681-7. [http://dx.doi.org/10.1016/0360-3016(80)90223-0] [PMID: 7451273]

[38] Amin B, Elahi MA, Shahzad A, Parle E, McNamara L, O'Halloran M. An insight into bone dielectric properties variation: A foundation for electromagnetic medical devices. 2018 EMF-Med 1st World Conference on Biomedical Applications of Electromagnetic Fields (EMF-Med). 10-13 September 2018; Split, Croatia. 2018. [http://dx.doi.org/10.23919/EMF-MED.2018.8526050]

[39] Ali U. Design and SAR analysis of wearable antenna on various parts of human body, using conventional and artificial ground planes. J Electr Eng Technol 2017; 12(1): 317-28. [http://dx.doi.org/10.5370/JEET.2017.12.1.317]

[40] Balarami Reddy BN, Sandeep Kumar P, Rama Rao T, Tiwari N, Balachary M. Design and analysis of wideband monopole antennas for flexible/wearable wireless device applications. Prog Electromagn Res M Pier M 2017; 62: 167-74. [http://dx.doi.org/10.2528/PIERM17092107]

[41] Singh N. A snapshot of patients' awareness of radiation dose and risks associated with medical imaging examinations at an Australian radiology clinic. Radiography 2017; 23(2): 94-102. [http://dx.doi.org/10.1016/j.radi.2016.10.011]

[42] Lin EC. Radiation risk from medical imaging. Mayo Clin Proc 2010; 85(12): 1142-6. [http://dx.doi.org/10.4065/mcp.2010.0260] [PMID: 21123642]

[43] David JM, Sachin J, John BK, Sharad G. Diagnostic medical imaging in pediatric patients and subsequent cancer risk. Acad Radiol 2017; 24(11): 1456-62. [http://dx.doi.org/10.1016/j.acra.2017.05.009]

[44] Li ML, Zhang HF, Maslov K, Stoica G, Wang LV. Improved *in vivo* photoacoustic microscopy based on a virtual-detector concept. Opt Lett 2006; 31(4): 474-6. [http://dx.doi.org/10.1364/OL.31.000474] [PMID: 16496891]

[45] Matrone G, Savoia AS, Caliano G, Magenes G. The delay multiply and sum beamforming algorithm in ultrasound B-mode medical imaging. IEEE Trans Med Imaging 2015; 34(4): 940-9. [http://dx.doi.org/10.1109/TMI.2014.2371235] [PMID: 25420256]

[46] Jeon S, Park EY, Choi W, Managuli R, Lee K, Kim C. Real-time delay-multiply-and-sum beamforming with coherence factor for *in vivo* clinical photoacoustic imaging of humans. Photoacoustics 2019; 15: 100136. [http://dx.doi.org/10.1016/j.pacs.2019.100136] [PMID: 31467842]